Electrodisintegration of ^{3}He[†]

P. T. Kan, G. A. Peterson, D. V. Webb, and Z. M. Szalata

Department of Physics and Astronomy, University of Massachusetts, Amherst, Massachusetts 01002

J. S. O'Connell, S. P. Fivozinsky, J. W. Lightbody, Jr., and S. Penner

Center for Radiation Research, National Bureau of Standards, Washington, D. C. 20234

(Received 23 June 1975)

The continuum spectra of ^{3}He have been measured up to excitation energies of 40 MeV by means of inelastic electron scattering. Incident electron beam energies between 60 and 120 MeV were used, corresponding to a momentum transfer range of 0.3 fm^{-1} to 1.1 fm^{-1}. Scattered electrons were observed at two angles, 92.6° and 127.7°. The radiation corrected spectra and the form factors are presented, and compared with calculations based on a zero-range approximation. In this model, the sharp rise from the $p+d$ threshold previously reported may be identified as a $^2S \to {}^2S$ Coulomb monopole transition.

NUCLEAR REACTIONS ^{3}He(e, e'), $E_x = 0$–40 MeV; measured $\sigma(E; \theta)$; $\theta = 92.6°$ and 127.7°. Comparison between radiation-corrected spectra and zero-range model calculations; multipole decomposition.

I. INTRODUCTION

This paper reports an experiment in which the continuum spectra of electrons inelastically scattered from ^{3}He have been measured up to excitation energies of 40 MeV. Upon sufficient transfer of energy from the incident electron, the ^{3}He nucleus could undergo either a two-body breakup, $e + {}^3\text{He} \to e' + p + d$, or a three-body breakup, $e + {}^3\text{He} \to e' + p + p + n$, with thresholds at 5.5 and 7.7 MeV, respectively. Since only the electrons were detected, and not the outgoing nucleons, the sum of these breakup cross sections was measured. The three-momentum transferred to the nucleus q was in the range from 0.3 to 1.1 fm^{-1}. In previous ^{3}He(e, e') experiments Hughes, Yearian, and Hofstadter[1] made measurements in a higher range of q, Frosch *et al.*[2] were concerned mainly with the threshold region, Johansson[3] did a coincidence experiment, and Chertok *et al.*[4] primarily measured transverse continuum transitions in a 180° experiment. The present experiment was performed with higher resolution and lower background than the previous electron-scattering experiments on ^{3}He.

There have been many measurements of the two-body photodisintegration[5] of ^{3}He and its inverse.[6] There have been fewer of the difficult three-body photodisintegration measurements.[7] Fundamentally, our experiment differs from photodisintegration experiments in that we have measured a sum of two- and three-body cross sections, and secondly, in photonuclear reactions the momentum transfer q is uniquely related to the excitation energy k, whereas in electron scattering these two quantities can be varied indepen-

dently. By measuring the cross section at a given k, and by varying q, information about the radial dependence of the nuclear transition density can be obtained, and the transition multipolarity can sometimes be determined. In photodisintegration, the multipolarity is primarily electric dipole,[5,6] whereas in electrodisintegration other multipolarities can contribute strongly if appropriate momentum transfers and kinematic conditions are chosen.[8]

For the q range of this experiment it was found that the form factors were of similar shape throughout the excitation region except for the energy interval between the two- and three-body breakup thresholds, where a broad Coulomb monopole contribution was found.[9]

We have calculated the cross sections for the electrodisintegration of ^{3}He in the zero-range model.[10] The calculations give reasonably good agreement with the measured spectra of the present experiment. The calculated dominant transitions are $C0$, $C1$, $M2$, and $C2$. In particular, the sharp rise in the cross section from the two-body threshold may be explained as a $^2S \to {}^2S$ Coulomb monopole transition.

II. EXPERIMENTAL METHOD

The 140 MeV linear accelerator of the National Bureau of Standards was used to provide electron beams of about 10 μA average currents. Energy slits in the magnetic beam transport system defined the energy spread of the electrons incident on the target to 0.25% of the incident energy E_0. Data were taken for $E_0 = 60$, 75, 90, and 110 MeV at a scattering angle θ of 92.6° and for $E_0 = 120$

MeV with $\theta = 127.7°$.

An "O"-ring sealed rectangular gas target cell[11] with dimensions of 14 cm × 8 cm × 4 cm was pressurized to about 10 atm. The entrance window was made of 0.0015 cm Havar[12] foil, the exit window of 0.0026 cm stainless steel foil, and the side window of 0.013 cm stainless steel foil. Since no massive portion of this rather large target cell was within the solid angle for observing electrons scattered from the ^{3}He gas, and since the entrance and exit foils were thin, backgrounds were relatively small. The temperature and pressure of the target were continually monitored. It was found that there was no detectable dependence of charge-normalized counts upon beam current, temperature, or pressure for this sealed-off target. The scattered electrons which passed through the side window were momentum analyzed with a double-focusing magnetic spectrometer,[13] and were detected by a 48 channel triple coincidence hodoscope[14] in the spectrometer focal plane. In order to reduce the neutron background, a Plexiglas Čerenkov counter replaced the scintillator normally employed as the backup detector. In some instances, the background was reduced by as much as a factor of 5 by use of the Čerenkov counter. The details of the on-line data collection electronics have been given elsewhere.[14,15] The primary beam-current monitor was a Faraday cup.[16] As a result of losses due to multiple scattering in the target, the Faraday cup did not intercept 100% of the incident electrons. An additional monitor, a non-intercepting toroidal ferrite, was located upstream of the target so that the beam current losses could be measured. These losses were less than 1% of the incident beam current at the energies used in this experiment.

The raw data were corrected for spectrometer dispersion, detector efficiency variations, and dead-time losses in the counting circuits. The background arising from the target cell was measured by using an identical evacuated cell, and was found to be no larger than the background with no target cell in the beam. Figure 1 shows two typical spectra of scattered electrons.

III. ANALYSIS

Radiative corrections were applied to the data before the cross sections were extracted. The elastic-scattering cross section was obtained by integrating the elastic-scattering peak to a cutoff energy of 1 MeV and applying Schwinger,[17] thick-target bremsstrahlung,[18] and ionization straggling[19] corrections. The corrected peak area was normalized to the sum of the cross sections for elastic scattering from the charge and magnetic dipole
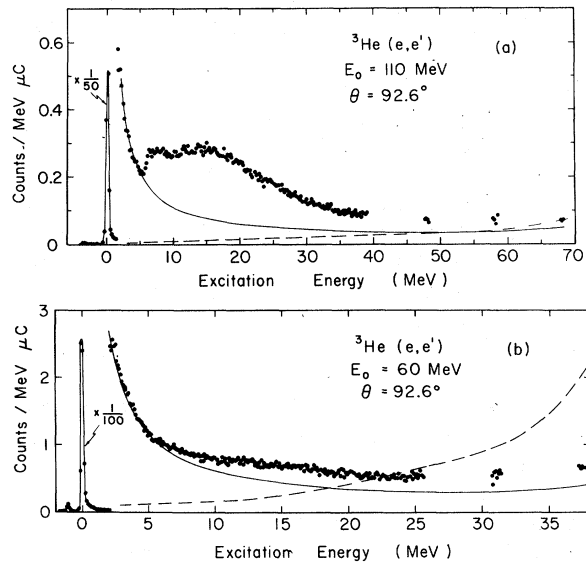

FIG. 1. Spectra of electrons scattered from (a) ^{3}He at incident energies of 110 MeV and (b) 60 MeV. The solid line is a calculated elastic radiation tail (see Sec. III) and the dashed line is the empty target background which has been subtracted from the data.

moment of ^{3}He. The charge elastic-scattering cross section was calculated with the phase-shift code of Rawitscher and Fischer.[20] The magnetic elastic-scattering cross section was calculated[21] in the Born approximation. Coulomb distortion effects in the case of magnetic scattering were assumed to be the same as for charge scattering. Gaussian charge and magnetization distributions[22] with rms radii of 1.88 and 1.95 fm, respectively, were used in the calculations of the elastic-scattering cross sections.

Electrons elastically scattered from a nucleus, but degraded in energy by bremsstrahlung emission and by collisions with atomic electrons give rise to the so-called elastic radiation tail at energies less than the elastic peak energy. The radiation tail cross section formulas of Maximon and Isabelle[23] were used to account for photon emission during the nuclear elastic scattering. Their formulas are based upon an integration of the Bethe-Heitler bremsstrahlung cross section over all photon emission angles. A Gaussian elastic charge form factor[22] with a ground state rms radius of 1.88 fm was used in the calculation. Contributions to the radiation tail from thick-target radiative processes and from electron-electron scattering[19] were included.

A comparison was made between a measured spectrum of electrons scattered from ^{4}He for $E_0 = 90$ MeV and $\theta = 92.6°$, and a calculated elastic radiation tail, as shown in Fig. 2. This compari-

son provides a good check of the calculations and experiment since the elastic radiation tail is the only source of scattered electrons for the first 19 MeV of the ^{4}He spectrum. A Gaussian charge distribution with an rms radius[24] of 1.63 fm was used for ^{4}He in this calculation. The difference between the data and the calculated radiation tail is due to instrumental background resulting from the scattering of electrons from the spectrometer vacuum chamber into the detector array. For all of the ^{3}He runs, the calculated tails were normalized by a multiplicative factor to fit the data just before the two-body threshold and then subtracted from all points in the spectra, thus largely removing the instrumental background. The multiplicative factor increased from 1.05 to 1.23 as E_0 was decreased from 120 to 60 MeV.

The continuum ^{3}He data were then subjected to inelastic radiative unfolding. The spectra were first divided into 1 MeV intervals, each of which contained 10 energy bins. Within a given 1 MeV interval, the mean inelastic Schwinger, Bethe-Heitler, and ionization corrections[25] were used. These corrections were applied to the counts in the first bin at the highest electron energy at which the unfolding began. The inelastic radiation tail[26] from this bin was calculated and subtracted from all subsequent bins. This procedure was repeated for all subsequent bins in the spectrum. Only the peaking term in Ref. 26 was used in the calculation of the inelastic radiation tail, and the inelastic form factor was assumed to be proportional to q^2 as for an electric dipole transition. Various expressions for the form factor were found to produce only small differences in
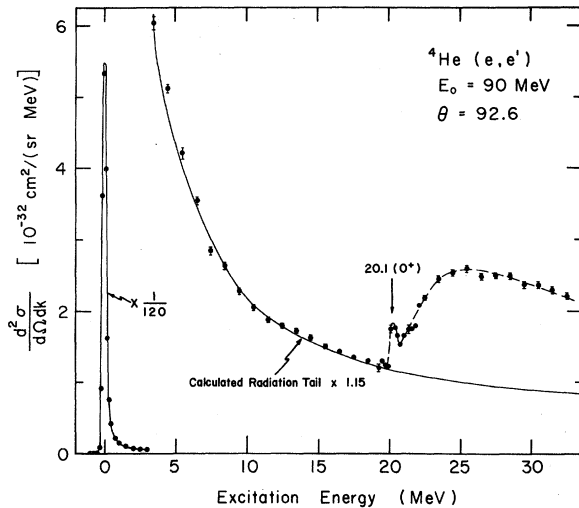
the continuum radiation corrections at large excitation energies.

IV. EXPERIMENTAL RESULTS

The continuum spectra after radiative unfolding, as shown in Fig. 3, are characterized by a steep rise from the two-body threshold at 5.5 MeV, followed by a change of slope just before the three-body threshold at 7.7 MeV. Several more data points were taken beyond 40 MeV excitation for the $E_0 = 110$, 90, and 75 MeV runs in order to check the asymptotic behavior of the spectra. These points show a monotonically decreasing behavior of the cross sections at large excitation energies. A systematic uncertainty of $\pm 5\%$ of the continuum cross sections near threshold is estimated to include uncertainties in the elastic cross sections, background subtraction, and in the unfolding procedure. This uncertainty increases with excitation energy as the target-cell background increases. The background contribution of the empty cell for the $E_0 = 60$ MeV spectrum, as shown in Fig. 1(b), becomes very large at low scattered electron energies where multiple-scattering events become the dominant process. There are additional multiple-scattering events in the ^{3}He gas which are not observed in the empty-cell spectrum. Systematic errors resulting from the empty-target background subtraction for the $E_0 = 60$ MeV measurements have been estimated by assuming the continuum cross sections to have the same shape at large excitation energies as for the $E_0 = 75$ MeV spectrum. This uncertainty becomes as large as 30% at 22 MeV excitation for the $E_0 = 60$ MeV spectrum.

The form factors measured in this experiment are given in Table I. We define the square of the continuum form factor to be

$$| F(q,k) |^2 = \frac{1}{\sigma_{\text{Mott}}} \left\langle \frac{d^2\sigma}{d\Omega dk} \right\rangle , \qquad (1)$$

where

$$\sigma_{\text{Mott}} = \left(\frac{Ze^2}{2E_0} \right)^2 \frac{\cos^2(\tfrac{1}{2}\theta)}{\sin^4(\tfrac{1}{2}\theta)} \left(1 + \frac{2E_0}{Mc^2} \sin^2(\tfrac{1}{2}\theta) \right)^{-1}$$

is the Mott cross section for scattering from a point nucleus of charge Ze and mass M, and $\langle d^2\sigma/d\Omega dk \rangle$ is an average over 1 MeV intervals of the measured cross section.

V. MODEL CALCULATIONS

We have calculated the Coulomb form factors F_C and the transverse form factors F_T, for ^{3}He breakup using simple wave functions as a guide to interpreting the multipole components of the

FIG. 2. Comparison of the elastic radiation tail (solid line) with a spectrum of electrons scattered from ^{4}He. The empty-target background has been removed.

TABLE I. Measured continuum form factors $F^2(q,k)$ averaged over 1 MeV intervals. The numbers in parentheses are the percentage standard deviations which include 5% systematic uncertainties for all spectra except for the $E_0 = 60$ MeV spectrum, in which 5–30% systematic errors have been included.

k (MeV)	$E_0 = 120$ MeV q^2 (fm^{-2})	$F^2(q,k)$ (10^{-3} MeV^{-1})	$E_0 = 110$ MeV q^2 (fm^{-2})	$F^2(q,k)$ (10^{-3} MeV^{-1})	$E_0 = 90$ MeV q^2 (fm^{-2})	$F^2(q,k)$ (10^{-3} MeV^{-1})	$E_0 = 75$ MeV q^2 (fm^{-2})	$F^2(q,k)$ (10^{-3} MeV^{-1})	$E_0 = 60$ MeV q^2 (fm^{-2})	$F^2(q,k)$ (10^{-3} MeV^{-1})
6.0	1.058	3.12(12.2)	0.595	2.23 (6.3)	0.395	1.96(11.3)	0.271	1.20(12.9)	0.170	0.56(25.1)
7.0	1.048	5.68 (9.4)	0.590	4.02 (7.6)	0.390	3.23 (8.2)	0.268	1.93 (9.8)	0.167	1.03(14.3)
8.0	1.039	6.86 (9.0)	0.584	4.78 (7.1)	0.386	3.47 (8.0)	0.264	2.16 (9.0)	0.165	1.53(11.4)
9.1	1.029	7.66 (9.1)	0.578	4.64 (7.4)	0.381	3.89 (7.2)	0.260	2.43 (8.3)	0.162	1.64(10.9)
10.1	1.020	9.01 (8.0)	0.573	5.05 (7.6)	0.377	4.18 (7.1)	0.257	2.66 (8.2)	0.159	1.65(10.8)
11.2	1.010	9.68 (8.6)	0.568	5.74 (7.3)	0.373	4.68 (7.3)	0.253	2.84 (8.0)	0.156	2.01(10.7)
12.2	1.001	11.24 (9.3)	0.562	6.09 (7.2)	0.368	5.00 (7.5)	0.250	3.20 (7.7)	0.154	2.30(10.3)
13.2	0.992	13.26 (8.6)	0.557	6.37 (7.1)	0.364	4.82 (8.0)	0.246	3.23 (7.6)	0.151	2.28(10.9)
14.2	0.983	13.69(10.3)	0.552	6.58 (7.0)	0.360	4.84 (7.9)	0.243	3.15 (7.7)	0.149	2.08(12.7)
15.3	0.974	13.36(11.0)	0.547	6.76 (7.0)	0.356	4.90 (7.9)	0.240	3.09 (8.0)	0.146	2.08(14.6)
16.4	0.965	12.79(11.6)	0.542	6.49 (7.0)	0.352	4.79 (8.0)	0.237	2.57 (8.1)	0.144	2.02(15.8)
17.5	0.956	14.37(13.2)	0.537	6.21 (7.1)			0.234	2.41 (8.6)	0.142	2.07(19.5)
18.3			0.532	6.26 (7.2)			0.230	2.22 (9.3)	0.139	1.83(21.5)
19.3			0.527	5.74 (7.1)			0.228	2.10 (9.6)	0.137	2.08(25.5)
20.3			0.522	5.44 (7.0)			0.224	1.98 (9.9)	0.135	1.94(29.8)
21.4			0.517	4.91 (7.9)			0.222	1.84(10.5)	0.133	1.70(36.0)
22.4			0.513	4.52 (8.8)			0.219	1.64(11.5)	0.130	1.82(45.1)
23.4			0.508	4.20 (8.9)			0.216	1.83(10.9)		
24.4			0.503	4.37 (9.0)			0.213	1.52(12.4)		
25.5			0.499	3.68 (8.9)			0.210	1.54(11.9)		
26.6			0.494	3.35(10.0)			0.208	1.50(12.5)		
27.6			0.490	2.86(10.8)			0.205	1.30(15.3)		
28.7			0.485	2.73(10.8)						
29.7			0.481	2.35(11.4)						
30.8			0.477	2.15(11.1)						

reaction. Zero-range-type wave functions have previously been used in $p+d$ and $p+p+n$ photo-disintegration calculations[10] in the excitation region up to 40 MeV. These wave functions mimic the asymptotic three-nucleon behavior with sufficient accuracy to give the energy dependence of two- and three-body electric dipole photodisintegration cross sections. The momentum transfers of the present experiment are low enough so that the predictions of this model still may be reliable.

The experimental form factor defined in Eq. (1) is given by

$$|F(q,k)|^2 = \frac{q_\mu^4}{q^4} |F_C(q,k)|^2$$

$$+ \left(\frac{q_\mu^2}{2q^2} + \tan^2(\tfrac{1}{2}\theta)\right)|F_T(q,k)|^2 ,$$

where

$$|F_C|^2 = Z^{-2}\left|\left\langle \Psi_k \left| \sum_i e_i \exp(i\vec{q}\cdot\vec{r}_i) \right| \Psi_0 \right\rangle\right|^2$$

and

$$|F_T|^2 = Z^{-2}\left[\left|\left\langle \Psi_k \left| \sum_i \frac{e_i\vec{q}\times\vec{p}_i}{M} \exp(i\vec{q}\cdot\vec{r}_i) \right| \Psi_0 \right\rangle\right|^2\right.$$

$$\left. + \left|\left\langle \Psi_k \left| \sum_i \frac{\mu_i\vec{\sigma}_i\times\vec{q}}{2M} \exp(i\vec{q}\cdot\vec{r}_i) \right| \Psi_0 \right\rangle\right|^2\right].$$

The ^{3}He ground state is taken as

$$\Psi_0(r,\rho) = \frac{(4\gamma\alpha)^{1/2}}{4\pi}\frac{\exp(-\gamma r - \alpha\rho)}{r\rho}\chi_{\frac{1}{2}0} ,$$

where $\vec{r}$ is the coordinate between a pair of nucleons and $\vec{\rho}$ the coordinate of the third nucleon relative to the center of mass of the pair. The spin-$\frac{1}{2}$ function χ has the proton pair in a spin singlet. The continuum wave functions for $p+d$ breakup are for s wave:

$$\Psi_{\alpha p}(r,\rho) = \phi_D(r)\frac{\sin(p\rho+\delta_p)}{p\rho}\chi_{S1} ,$$

where

$$p\cot\delta_p = -\alpha_S ;$$

and for $L>0$:

$$\Psi_{\alpha p} = \phi_D(r)4\pi i^L j_L(p\rho)Y_{LM}^*(\hat{p})Y_{LM}(\hat{\rho})\chi_{S1} ,$$

where $\phi_D(r)$ is the zero-range deuteron wave function

$$\phi_D(r) = \left(\frac{2\gamma}{4\pi}\right)^{1/2}\frac{e^{-\gamma r}}{r}$$

and χ_{S1} is the $p+d$ doublet ($S=\frac{1}{2}$) or quartet ($S=\frac{3}{2}$) spin function. For $p+p+n$ breakup, the continuum wave functions are for s wave:

$$\Psi_{tp}(r,\rho) = \frac{\sin(tr+\delta_t)}{tr}\frac{\sin(p\rho+\delta_p)}{p\rho}\chi_{Ss} ,$$

where

$$t\cot\delta_t = -\gamma_s$$

and

$$p\cot\delta_p = -\alpha_S ;$$

and for $L>0$:

$$\Psi_{tp}(r,\rho) = \frac{\sin(tr+\delta_t)}{tr}4\pi i^L j_L(p\rho)Y_{LM}^*(\hat{p})Y_{LM}(\hat{\rho})\chi_{Ss}$$

where s is the pair spin and S the total spin.

Note that we assume that there is always a pair of nucleons in a relative s wave in the final state. This pair determines the $\vec{r}$ coordinates in the ground state.

These wave functions are not solutions of the three-nucleon Schrödinger equation using a two-nucleon potential. However, they are consistent in the sense that each partial wave is orthogonal to its bound state. The s-wave radial orthogonality is particularly important for monopole transitions.

The bound-state parameters γ and α are chosen to give reasonable fits to the electric dipole photo-disintegration cross section. The values $\gamma = 0.232$ fm^{-1} and $\alpha = 0.420$ fm^{-1} give a calculated three-nucleon photodisintegration cross section that agrees in shape and magnitude with the photodisintegration data. The calculated $p+d$ photodisintegration cross section reproduces the photon energy dependence of $\sigma_\gamma(k)$, but underestimates the magnitude of the cross section by a factor of 3. This fault is due to the use of oversimplified factored wave functions and to the lack of coupling of the two- and three-body final states as required by Faddeev theory. We multiply the $L\geq 1$ two-body model amplitudes by $3^{1/2}$ in the hope that once these amplitudes are normalized at the photon point $q=k$, the momentum dependence of the transition form factors will be given correctly. The two-body monopole amplitude is exempt from this normalization in order to preserve the monopole sum rule, as are all the $p+p+n$ amplitudes, since they are in agreement with the photodisintegration data.[5]

The final state s-wave parameters approximate the nucleon-deuteron and nucleon-nucleon scattering lengths for the appropriate spins.

$$\alpha_{1/2} = \alpha = (2.38 \text{ fm})^{-1}, \quad \alpha_{3/2} = (6.4 \text{ fm})^{-1} ,$$

$$\gamma(np)_1 = \gamma = (4.31 \text{ fm})^{-1} ,$$

$$\gamma(np)_0 = (-24 \text{ fm})^{-1}, \quad \gamma(pp)_0 = (-7.8 \text{ fm})^{-1} .$$

Using these wave functions the form factors

are calculated following the method outlined in Refs. 27 and 28. The Coulomb transitions $C0$, $C1$, and $C2$ dominate the cross section at the scattering angles of the present experiment. The relatively small transverse contribution is mainly two-body $M2$. The cross sections are plotted in Fig. 3, and a form factor in Fig. 4. A decom-
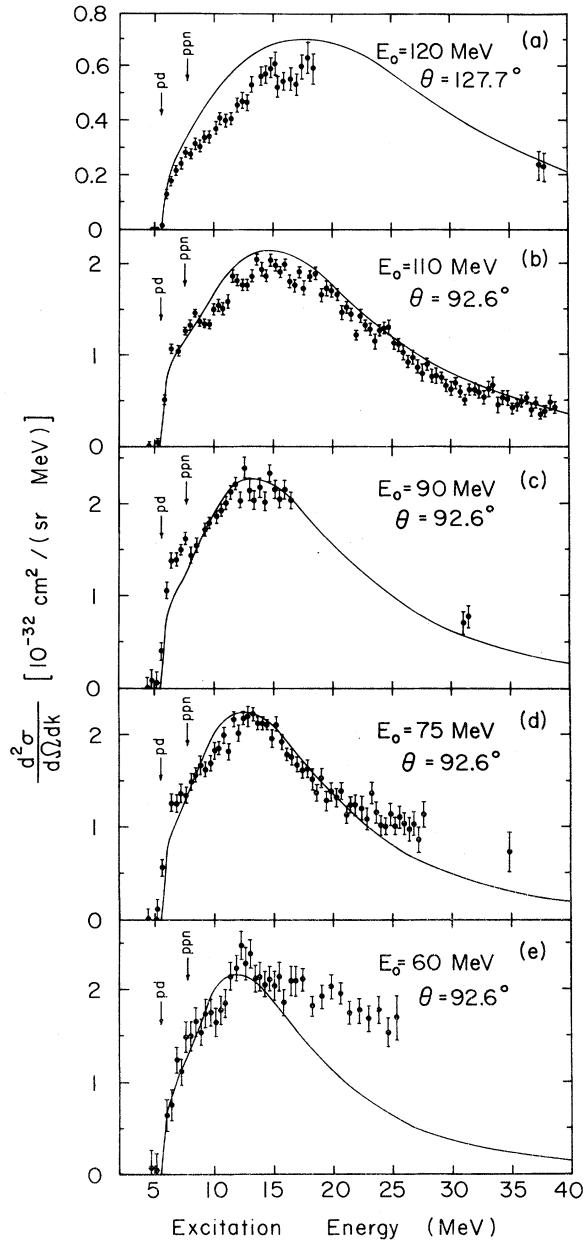

FIG. 4. Form factor $F^2(q,k)$ at an excitation energy of 15 MeV. Systematic uncertainties of $\pm 5\%$ have been included in all of the data points except the point at $q = 0.382$ fm^{-1}, where a systematic error of $\pm 10\%$ has been estimated. The solid curve is the zero-range model form factor.

FIG. 3. Radiatively unfolded cross sections. The notations pd and ppn indicate the two- and three-body breakup thresholds, respectively. In each graph, the solid curve is the calculated result in the zero-range approximation (see Sec. V).
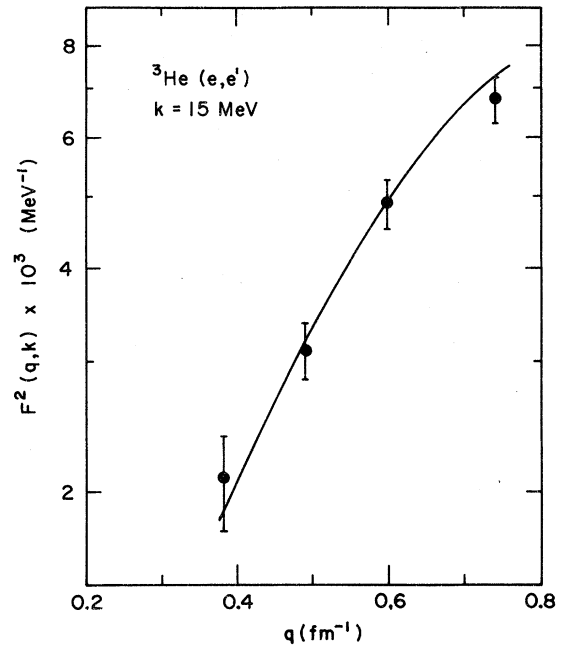
position into two- and three-body multipoles is given in Fig. 5.

VI. DISCUSSION AND CONCLUSIONS

The excitation cross sections and form factors of Figs. 3 and 5 show two interesting features: the rapid rise of the cross sections from the p $+d$ threshold at 5.5 MeV, and then the slower rise to a peak near 15 MeV followed by a monotonically decreasing high energy tail. We interpret the threshold behavior as a monopole excitation by the Coulomb operator. The model calculation for this $^2S \rightarrow {}^2S$ transition gives reasonable agreement with the data as a function of k and q. Coulomb monopole ($C0$) strength is expected[29] at the one-particle separation threshold in ^{2}H, ^{3}H, ^{3}He, and ^{4}He isotopes. In ^{4}He this strength is concentrated into a 0^+ resonant level.[30] For ^{3}He however, it appears that the final-state interaction between the proton and the deuteron is not strong enough to form a quasistationary state of narrow width. The model cross section has a full width at half maximum of 5 MeV for the two-body monopole transition.

In a previous analysis[9] of this data, the $C1$ contribution in the threshold region was obtained from

photoreaction results, by assuming the C1 transition radius to equal the ground-state charge radius. The present calculation indicates that the effective C1 transition radius is much larger than this estimate. However, because of the importance in the calculation of multipole components other than C1, the total non-C0 strength in the threshold region is not very different from what was used in Ref. 9 in order to extract the monopole strength. The monopole matrix element given in Ref. 9 applies only to the 5.5 to 8.5 MeV excitation region, not to the total monopole strength which, according to the present calculation, is spread over a wide range of excitation.

The region of the 15 MeV peak is composed of roughly equal parts of two-body C1, C2, and M2, and three-body C1 according to the model. The same M2 strength ($^2S - {}^2P + {}^4P$) accounts for most of the 180° cross section in the experiment of Chertok *et al.*[4] Our calculated M1 strength is small in comparison to the M2.

ACKNOWLEDGMENTS

We wish to acknowledge the valuable assistance of Dr. Frank J. Kline in the installation of the Cerenkov counter. We also appreciate the services provided by the National Bureau of Standards linac crew and by the University of Massachusetts Computing Center.
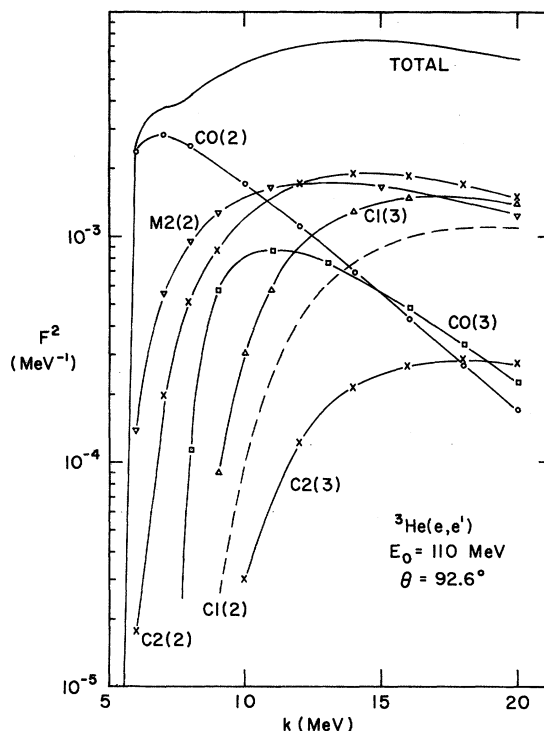

FIG. 5. Multipole decomposition of the form factor by using the zero-range model wave functions. The number 2 or 3 in parentheses denotes the two- or three-body breakup mode.

[1]E. B. Hughes, M. R. Yearian, and R. Hofstadter, Phys. Rev. **151**, 841 (1966).

[2]R. F. Frosch, H. L. Crannell, J. S. McCarthy, R. E. Rand, R. S. Safrata, L. R. Suezle, and M. R. Yearian, Phys. Lett. **24B**, 54 (1967).

[3]A. Johansson, Phys. Rev. **136**, B1030 (1964).

[4]B. T. Chertok, E. C. Jones, W. L. Bendel, and L. W. Fagg, Phys. Rev. Lett. **23**, 34 (1969); E. C. Jones, Ph.D. thesis, American University, 1973 (unpublished).

[5]G. Ticcioni, S. N. Gardner, J. L. Matthews, and R. O. Owens, Phys. Lett. **46B**, 369 (1973); C. C. Chang, W. R. Dodge, and J. J. Murphy, II, Phys. Rev. C **9**, 1300 (1974); N. M. O'Fallon, J. L. Koester, and J. H. Smith, *ibid.* C **5**, 1926 (1972); V. N. Fetisov, A. N. Gorbunov, and A. T. Varfolomeev, Nucl. Phys. **71**, 305 (1965); J. R. Stewart, R. C. Morrison, and J. S. O'Connell, Phys. Rev. **138**, B372 (1965); S. K. Kundu, Y. M. Shin, and G. D. Wait, Nucl. Phys. **A171**, 384 (1971); D. M. Skopik, J. J. Murphy, II, Y. M. Shin, K. F. Chong, and E. L. Tomusiak, Phys. Rev. C **11**, 693 (1975).

[6]G. M. Griffiths, E. A. Larson, and L. P. Robertson, Can. J. Phys. **40**, 402 (1962); W. Wölfi, R. Bösch, J. Lang, R. Müller, and P. Marmier, Helv. Phys. Acta **40**, 946 (1967); J. L. Matthews, T. Kruse, M. E. Williams, R. O. Owens, and W. Savin, Nucl. Phys. **A223**, 221 (1974).

[7]B. L. Berman, S. C. Fultz, and P. F. Yergin, Phys. Rev. C **10**, 2221 (1975); H. M. Gerstenberg and J. S. O'Connell, Phys. Rev. **144**, 834 (1966); V. N. Fetisov, A. N. Gorbunov, and A. T. Varfolomeev, Nucl. Phys. **71**, 305 (1965).

[8]T. de Forest, Jr., and J. D. Walecka, Advan. Phys. **15**, 1 (1966).

[9]P. T. Kan, G. A. Peterson, D. V. Webb, Z. M. Szalata, S. P. Fivozinsky, J. W. Lightbody, Jr., and S. Penner, Phys. Rev. Lett. **34**, 899 (1975).

[10]J. M. Knight, J. S. O'Connell, and F. Prats, Phys. Rev. **164**, 1354 (1967).

[11]D. V. Webb, G. A. Peterson, Z. M. Szalata, and P. T. Kan, Nucl. Instrum. Methods **120**, 359 (1974).

[12]The Havar foil was obtained from Hamilton Precision Metals, Lancaster, Pa. 17604, and was composed of 42.5% cobalt, 13.0% nickel, 20.0% chromium, 17.9% iron, and traces of other elements.

[13]S. Penner and J. W. Lightbody, Jr., in *Proceedings of the International Symposium on Magnet Technology, Stanford, California, 1965*, edited by H. Brechna and

M. S. Gordon (National Bureau of Standards, U. S. Dept. of Commerce, Washington, D. C., 1966), CONF-650922, p. 154.

[14]J. K. Whittaker, IEEE Trans. Nucl. Sci. 19, 444 (1972).

[15]S. Penner, National Bureau of Standards, Technical Note No. 532, 1970 (unpublished).

[16]J. S. Pruitt, Nucl. Instrum. Methods 100, 433 (1972).

[17]L. W. Mo and Y. S. Tsai, Rev. Mod. Phys. 41, 205 (1969).

[18]L. Heitler, Quantum Theory of Radiation (Oxford U. P., Oxford, England, 1954), 3rd ed., p. 377.

[19]B. Rossi, High Energy Particles (Prentice-Hall, Englewood Cliffs, N. J., 1952), Chap. 2.

[20]C. R. Fischer and G. H. Rawitscher, Phys. Rev. 135, B377 (1964).

[21]R. H. Pratt, J. D. Walecka, and T. A. Griffy, Nucl. Phys. 64, 677 (1965).

[22]J. S. McCarthy, I. Sick, R. R. Whitney, and M. R. Yearian, Phys. Rev. Lett. 25, 884 (1970).

[23]L. C. Maximon and D. B. Isabelle, Phys. Rev. 133, B1344 (1964).

[24]U. Erich, H. Frank, D. Haas, and H. Prange, Z. Phys. 209, 208 (1968).

[25]D. B. Isabelle and G. R. Bishop, Nucl. Phys. 45, 209 (1963).

[26]L. C. Maximon and D. B. Isabelle, Phys. Rev. 136, B674 (1964).

[27]D. R. Lehman, Phys. Rev. C 3, 1827 (1971).

[28]B. F. Gibson and G. B. West, Nucl. Phys. B1, 349 (1967).

[29]V. Z. Jankus, Phys. Rev. 102, 1586 (1956); T. Stovall and M. Danos, Phys. Lett. 7, 278 (1963).

[30]C. Werntz, Phys. Rev. 128, 1336 (1962).